Experimental and Theoretical Studies of $(CsI)_nCs^+$ Cluster Ions Produced by 355 nm Laser Desorption Ionization

F. A. Fernandez-Lima,[†] C. Becker,[†] K. Gillig,[†] W. K. Russell,[†] Marco Antonio Chaer Nascimento,[‡] and D. H. Russell*,[†]

Department of Chemistry, Texas A&M University, College Station, Texas, 77843 and Instituto de Química, Universidade Federal do Rio de Janeiro, Rio de Janeiro, 21949-900, Brazil

Received: May 28, 2008; Revised Manuscript Received: August 13, 2008

Collision cross-sections of gas-phase $(CsI)_{n\,=\,1-7}Cs^+$ cluster ions formed by pulsed-UV laser (355 nm) desorption ionization are measured by ion mobility-mass spectrometry. Experimental collision cross-sections are compared with calculated cross sections of candidate structures generated from a search for the lowest energy structures at the DFT/B3LYP/LACV3P** and MP2/LACVP3P** levels. The relative stabilities of these candidate structures are examined by IM-CID-MS, and the experimental results are compared to theoretical predictions. Analysis of $(CsI)_{n\,=\,1-7}Cs^+$ cluster ion dissociation energies shows that the lower fragmentation thresholds are observed for cluster ions with the lower predicted stability.

Introduction

Alkali halide clusters have received substantial attention in an effort to understand their physical and chemical properties (e.g., stability, bond length, and charge distribution) as the cluster size decreases and behaves less like bulk material. Mass spectrometry (MS) has been extensively used for experimental studies of alkali halide cluster ions to provide information on the cluster sizes and composition. Cluster ions can be produced by a variety of ion sources, e.g., sputtering[1−3] or laser desorption[4−7] of alkali halide surfaces, inert-gas condensation techniques,[8] and electrospray ionization.[9] Previous work has shown higher abundances of some cluster compositions, regardless of the ionization technique used,[1−9] which has been explained as increased stability of these cluster ions. Additionally, using time-of-flight measurements, Ens and co-workers showed there is not preferential formation of specific clusters at the time of formation,[10] i.e., the enhanced abundances observed in the mass spectra are attributed to a thermodynamic effect as a consequence of the cluster ion stabilities rather than to the ion production mechanism. Despite progress toward characterizing alkali halide cluster ions in MS experiments, no experimental evidence for specific cluster geometries have yet been obtained.

Ion mobility spectrometry (IMS) is a valuable technique for analysis of cluster ions and has been used to measure the mobility of atomic species, small covalent and metallic clusters, carbon clusters, and fullerenes.[11−22] Alkali halide cluster ions have also been analyzed by IMS.[23,24] However, in the case of CsI cluster ions, only the arrival time distributions have been reported.[23] Furthermore, measurements of the ion mobilities and collision cross-sections are necessary if cluster ion geometries are to be obtained.

From a theoretical point of view, alkali halide clusters are good candidates to evaluate the accuracy of theoretical predictions due to their elementary electronic and ionic bonding nature.[25−27] Theoretical calculations based on phenomenological pair potential models have been successful in describing the main characteristics of the alkali halide cluster and very useful for finding the local minima on the potential-energy surface.[25,28−32] With the advent of predictive ab initio methods, a series of alkali halide structures have been proposed, for example, the structures proposed by Aguado and co-workers using a perturbed-ion model[33−36] and Ochsenfeld and co-workers using the Møller−Plesset perturbation theory.[37,38] Understanding cluster stability is essential in deducing structural information. In previous work we have shown that theoretical cluster stabilities can be related to the ion abundances observed in the mass spectra and that ab initio calculations including electron correlation can provide an accurate description of the most stable candidate structures.[39−43]

Although studies of alkali halide ionic clusters have been reported,[1−9,23−38,44,45] a comprehensive and detailed characterization of the $(CsI)_nCs^+$ series has not been performed. Here, we report the first combined theoretical and experimental characterization of $(CsI)_{1-7}Cs^+$ cluster ions in terms of collision cross-sections and cluster stabilities. Cluster ions were produced by a pulsed UV laser (355 nm) and analyzed using ion mobility-collision-induced dissociation-mass spectrometry (LDI-IM-CID-MS). A search for the most stable candidate structures was performed using density functional theory (DFT) and Møller−Plesset (MP) perturbation theory. Different collisional activation regimes in the IM cell and in the CID interface were used to study the relative stabilities of cluster ions formed by LDI. Theoretical results of the relative stability of the cluster ions were compared with the experimental results (MS abundances and CID probabilities) in order to determine the most stable structures.

Experimental Methods

The experimental details of the LDI-IM-MS instrumentation and data acquisition used in this study have been described elsewhere.[46−48] Briefly, ions were desorbed from a CsI polycrystalline target inside an IM cell using a 355 nm Powerchip Nanolaser (JDS Uniphase Corp., Milpitas, CA) operating at a pulse rate of 300 Hz. The desorbed ions were separated according to their drift time in an IM cell maintained at a

* To whom correspondence should be addressed. E-mail: russell@mail.chem.tamu.edu.
[†] Texas A&M University.
[‡] Universidade Federal do Rio de Janeiro.

10.1021/jp8047086 CCC: $40.75
Published on Web 10/09/2008

TABLE 1: Lennard−Jones Pair Potential Parameters Used in the Ion−Neutral Collision Cross-Section Determination[a]

atom pair	σ (Å)	ε (meV)	R_{HS} (Å)
Cs−He	3.90	2.25	3.25
I−He	4.06	1.90	3.40
C−He	3.04 (3.06[b])	1.37 (1.34[b])	2.70 (2.70[b])
Si−He	3.60 (3.50[b])	1.90 (1.35[b])	3.05 (2.95[b])

[a] σ is the distance where the potential became positive, and ε is the well depth. R_{HS} is the hard-sphere radius for the EHSS model. The LJ equilibrium distance was determined at the MP2/LACV3P** level of optimization, and the LJ energy was determined from a single-point calculation at the MP2/LACV3P**/B3LYP/LACV3P** level. [b] Empirical values were taken from the fitting of IM spectra of C_{60} and small Si clusters.[51,55]

pressure of ~3.3 Torr of helium and field strength of 10−40 V cm^{-1} Torr^{-1}. To study the dissociation channels, ions exiting the IM cell were activated by collisional induced dissociation (CID) in the IM-MS interface and then focused into the ion source of an orthogonal time-of-flight mass spectrometer equipped with an electrostatic mirror (mass resolution of 1500−3000). Field strengths in the range of 20−120 V/cm were used in the CID region. In all experiments the temperature of the bath gas was ca. 300 K. The ion−neutral collision cross-sections (CCS) were reported according to the method described by Mason and McDaniel.[49] A fullerene mixture was used as a CCS reference.[50,51] The CCSs were measured using a laser power near the ion desorption threshold to minimize peak broadening of the arrival time distribution (ATD) due to space charge effects.[52] For comparison purposes, CID experiments were also performed on an Applied Biosystems 4700 Mass Spectrometer (Framingham, Ma).

Theoretical Methods

Theoretical calculations were performed to determine the most stable candidate structures of the $(CsI)_nCs^+$ ($n = 1-8$) cluster ions. The cluster ion structures were calculated using density functional theory (DFT) at the B3LYP/LACV3P** level and Møller−Plesset (MP) perturbation theory at the MP2/LACV3P** level. The LACV3P basis set is a triple-zeta contraction of the LACVP basis set[53] developed and tested at Schrödinger, Inc. (Portland, OR). Symmetry restrictions were not imposed in the process of geometry optimization. A vibration analysis was performed for all structures obtained at the levels of calculation used. All frequencies were found to be real, indicating that the optimized structures correspond to true minima in their respective potential-energy hypersurfaces. The frequencies were also used to compute the zero-point correction energy (ZPE) for all the optimized structures. Jaguar 6.0 software was used for the geometry optimization and vibrational analysis.[54]

Theoretical CCS values were calculated using the projection approximation (PA), exact hard-sphere scattering (EHSS), and trajectory Monte Carlo (TM) methods.[51,55] Lennard−Jones (LJ) pair potentials for the Cs−He and I−He were theoretically determined by averaging over different configurations of small cluster structures (Table 1). The LJ equilibrium distances were determined at the MP2/LACV3P**++ level, and the LJ total energies (including the zero-point energy correction) at the optimized geometries were determined from single-point calculations at the DFT/B3LYP/LACV3P**++ level (see Table 1). This methodology was tested by comparing the theoretically determined LJ interaction potentials for C−He and Si−He atom pairs with the empirical potentials reported from ion mobility experiments, and good agreement was observed [51,55] (results in Table 1). The Cs−He and I−He LJ interaction potentials were incorporated in the MOBCAL software for the CCS calculations.[51,55]

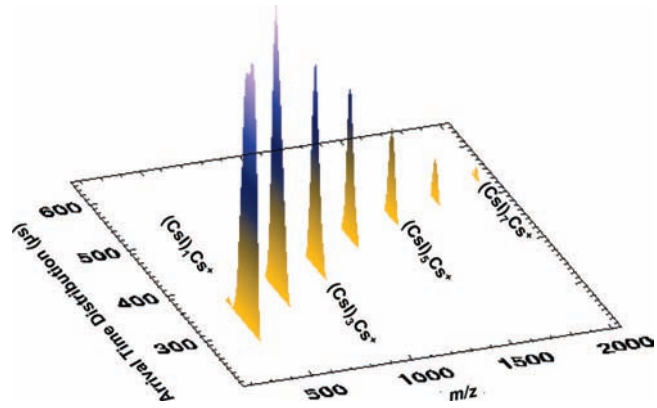

Figure 1. Three-dimensional ion mobility−time-of-flight plot of $(CsI)_{n=1-7}Cs^+$ cluster ions produced by 355 nm LDI for a field strength of 20 V cm^{-1} Torr^{-1} in the IM cell and 20 V/cm in the IM-CID-MS.

TABLE 2: Theoretical E_n and D_n Values Calculated at the DFT/B3LYP/LACV3P Level[a]**

structure	DFT/B3LYP/ LACV3P** results		theoretical ion−neutral collision cross-sections (Å^2)			experimental ion−neutral collision cross-sections (Å^2)
n	E_n (eV)	D_n (eV)	PA	EHSS	TM	IM-MS
0	−536.94	−0.26	33	33	–	32 ± 8
1	−1391.58	−0.25	70	72	67 ± 8	85 ± 13
2 I	−2245.95	0.04	90	95	98 ± 6	105 ± 11
2 II	−2245.92	0.07	108	113	117 ± 6	
2III	−2245.82	0.17	98	103	93 ± 6	
3 I	−3100.79	−0.15	113	121	125 ± 7	133 ± 10
3 II	−3100.21	0.42	127	136	138 ± 6	
4 I	−3955.12	0.17	134	145	148 ± 10	160 ± 11
4 II	−3955.06	0.23	127	137	138 ± 7	
5 I	−4810.07	−0.12	148	161	165 ± 10	169 ± 10
5 II	−4809.99	−0.04	154	167	172 ± 6	
5III	−4809.91	0.04	146	158	162 ± 9	
6 I	−5664.69	−0.09	160	175	181 ± 10	183 ± 8
6 II	−5664.57	0.03	172	191	196 ± 11	
7 I	−6519.52	−0.27	183	202	209 ± 10	203 ± 8
7 II	−6519.26	−0.01	185	204	208 ± 11	
8	−7373.88	0.03	197	218	223 ± 10	–

[a] The ion−neutral collision cross-sections (helium as a buffer gas) were calculated using the projection approximation (PA), the exact hard-sphere scattering (EHSS), and the trajectory Monte Carlo (TM) methods with the theoretically developed Lennard−Jones pair potential for Cs−He and I−He interactions. The mean values of the experimental ion−neutral collision cross-sections were determined from the LDI-IM-MS data. $E_{av}((CsI)_nCs^+) = -854.65n - 536.68$ (eV).

Results and Discussion

A three-dimensional IM-MS projection plot of the laser-generated ions from a CsI target is contained in Figure 1. A clear separation of $(CsI)_nCs^+$ cluster ions ($n = 1-7$) is observed in both the mass-to-charge and ion mobility domains. Seven cluster ions are observed in the LDI-IM-MS experiment, which is greater than those observed in previous LDI-TOFMS experiments ($n = 1-3$),[4,5] and may be related to the presence of the helium buffer gas in the source (~3.3 Torr) during the laser absorption/desorption process.[56] The ATD obtained under low-field conditions in the IM drift cell were used to calculate the CCSs of the $(CsI)_nCs^+$ cluster ions ($n = 1-7$).[57] The experimental CCS values are contained in Table 2. The CCS values can be described as a second-order polynomial function of the cluster size, n, $CCS(n) = 38.75 + 38.27n - 2.23n^2$, which can

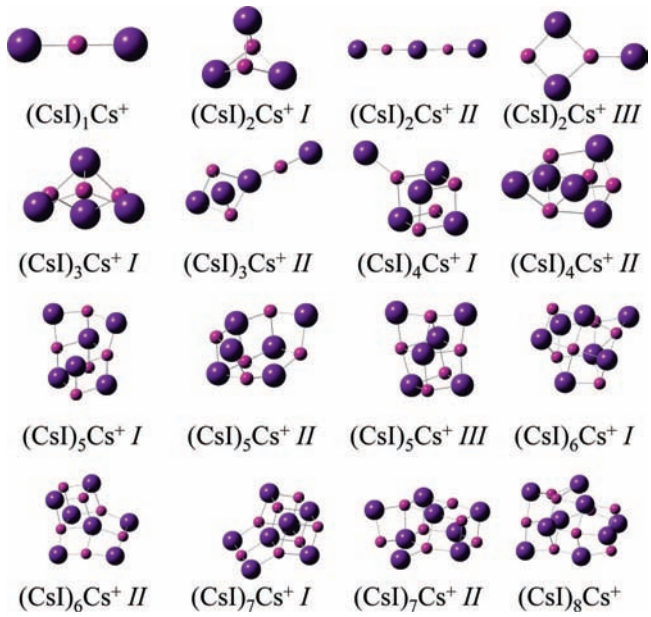

Figure 2. Optimized geometries of the $(CsI)_{n\,=\,1-8}Cs^+$ cluster ions at the DFT/B3LYP/LACV3P** calculation level. Structures labeled I are the most stable among the isomers.

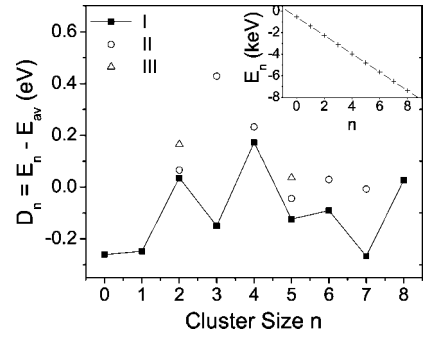

Figure 3. D-Plot: Deviation of the total energy (including the ZPE correction) as a function of the cluster size, n. (Inset) Total energy E_n as a function of the cluster size, n, ($E_{av}((CsI)_nCs^+) = -854.65n - 536.68$, in eV) is plotted. The connected dots correspond to the lowest energy isomers. The lower the D_n value, the higher the relative stability.

be helpful in future comparisons with other alkali halide cluster ions. For all cluster ions the ATD showed a Gaussian distribution profile, in agreement with previously reported ATD for $(CsI)_nCs^+$ ions.[23]

A search for candidate structures of the $(CsI)_nCs^+$ cluster ions was performed, and the total DFT energies (including the ZPE correction) are contained in Table 2. It is well known that DFT calculations on charged species may be in error due to the fact that for the present available DFT functionals the exchange energy does not exactly cancel the Coulombic self-interaction.[58] To check for possible inconsistencies, the DFT/B3LYP/LACV3P** optimized structures were also optimized at the MP2/LAVCV3P** level of calculation. Substantial changes were not observed in either the geometrical parameters or the relative stability of the clusters.

Despite the extensive search for potential candidate structures, three isomers for $n = 2$ and two isomers for $n = 3-7$ were found to be real minima at the DFT/B3LYP/LACV3P** level of calculation (see structures in Figure 2). Aguado et al. calculated the $(CsI)_{n\,=\,2-14}Cs^+$ cluster ion structures using an ab initio perturbed ion model.[36] However, at the DFT/B3LYP/LACV3P** and MP2/LACV3P** levels some of the structures previously proposed[36] show imaginary frequencies, i.e., they correspond to a false minima in the energy space and were not included in our results. Moreover, several new structures were obtained in our search (e.g., 3 II, 4 II, 6 II, 7 II, and 8). For $n > 3$, some structures show similarities with the crystalline structure of the CsI bulk material, e.g., structures 4 I, 4II, 5I, 5 III, 6 II, and 7 I still resemble a cubic structure. Although other candidate structures may exist, they probably belong to higher energy structures, which make them less probable to be experimentally observed due to the time scale of the IM-MS experiment, i.e., the higher the cluster energy content the higher the cluster instability.

Charge analysis, using the CHelpG algorithm,[59] showed that the $(CsI)_nCs^+$ cluster ions are assembled by electrostatic forces, where the individual charge on each Cs or I is proportional to the number of adjacent atoms. The Cs and I charges vary from +0.85 to +0.95 and −0.85 to −0.90, respectively; as the number of adjacent atoms increases, the probability of sharing an electron also increases, resulting in a net lower charge.

The theoretical CCSs of the $(CsI)_nCs^+$ ions are contained in Table 2. As the cluster size increases, long-range interactions and size effects become more important on the theoretical determination of the CCSs. For example, the CCSs obtained from the PA, EHSS, and TM methods are in better agreement for smaller cluster sizes than for larger cluster sizes, i.e., as the cluster size increases the PA method returns lower CCSs when compared to those of the EHSS and TM methods. The CCSs obtained by the EHSS method are smaller than those of the TM because of the longer range of the LJ potential compared to the hard-sphere model.[51,55] The overall consistency of the CCS results suggests that the parameters used in the theoretical CCS determination (Table 1) represent a good description of the ion−neutral interaction, at least as a first order of approximation. Although the CCSs obtained using EHSS and TM methods agree within error, the TM method was used for comparison with the experimental value because of the better description of the ion−He interaction when using a LJ potential interaction.[51,55] Comparison of the TM theoretical and experimental CCS values shows that the proposed structures are good candidates with the exception of $n = 4$, in which only the CCS of the more stable structure (4 I) shows close agreement with the experimental value.

To study the relative stability of the candidate structures contained in Figure 2 the Deviation plot (D-plot) methodology was used, whereby an energy criterion is considered by relating the total energy of a particular structure to the average energy across all the structures. A detailed discussion of the D-plot methodology can be found elsewhere.[39−43] Briefly, let $E_n(i)$ be the DFT total energy of the ith isomer of the $(CsI)_nCs^+$ cluster ion (including the ZPE correction) and $E_{av}[(CsI)_nCs^+]$ be the average energy of all n isomers. In a first order of approximation, the average energy shows a linear dependence on the cluster size (n) and is depicted in the inset of Figure 3: $E_{av}[(CsI)_nCs^+] = -854.65n - 536.68$, in eV units. For each isomer, the deviation energy is defined as $D_n(i) \equiv E_n(i) - E_{av}[(CsI)_nCs^+]$. Lower $D_n(i)$ values are associated with lower energy isomers and thus more stable structures.[39−43] The most relevant aspect of the D-plot is that the more stable isomers can be easily identified to facilitate the analysis of relative cluster stability. As a result, the candidate structures contained in Figure 2 are classified as follows: lowest energy structures (most stable isomers) are identified by the symbol "I" and higher energy structures with increasing roman numerals, i.e., "II" and "III".

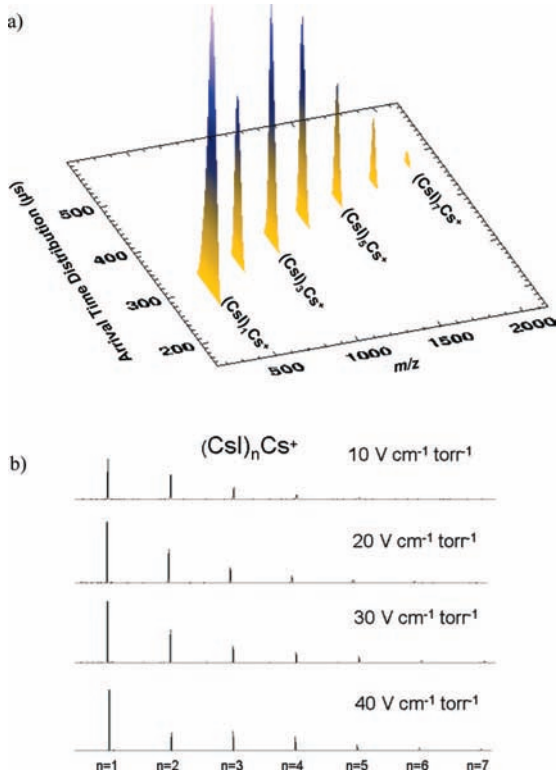

Figure 4. (a) Three-dimensional ion mobility−time-of-flight plot of $(CsI)_{n=1-7}Cs^+$ cluster ions produced by 355 nm LDI for a field strength of 40 V cm^{-1} $Torr^{-1}$ in the IM cell and 20 V/cm in the IM-CID-MS. (b) Relative abundances of the $(CsI)_{n=1-7}Cs^+$ ion signals as a function of the IM field strength. Notice the relative lower abundance of $(CsI)_2Cs^+$ cluster ion at 40 V cm^{-1} $Torr^{-1}$ in the IM cell.

The lowest energy structures are identified and connected with a straight line in Figure 3. A relatively high stability is observed for the odd-numbered cluster ions, e.g., $n = 3$ and 7, while cluster ions with $n = 2$ and 4 are less stable. The higher stabilities of $n = 3$ and 7 have been observed previously in MS experiments.[8] Inspection of Figures 2 and 3 shows that the cluster structures do not present any bonding pattern that could be related to the stability values, i.e., the charge distribution and bonding distances within the cluster do not present any abrupt change or trend that could be correlated with the stability values. This suggests that the higher stability is a consequence of the intrinsic cluster geometry that makes the electrostatic interaction between its constituents have a maximum for *n*-odd clusters, i.e., it is a consequence of the convolution of all the short- and long-range interaction between the cluster constituents.

The results of the stability analysis are in agreement with the observed IM experimental trends. That is, as the field strength in the IM cell is increased, a change in the relative abundance of the cluster sizes $n = 2$ and 3 is observed as a result of a multicollisional activation process (Figure 4a and 4b). For a field strength of 10−30 V cm^{-1} $Torr^{-1}$ in the IM cell, the ion abundance shows an exponential decrease as a function of the cluster size, *n*, where the abundance of $n = 2$ is higher than $n = 3$. At a field strength of 40 V cm^{-1} $Torr^{-1}$ (Figure 4a), the relative abundance of the $n = 3$ becomes larger than that of $n = 2$ as a consequence of their relative stabilities, i.e., $n = 3$ is more stable than $n = 2$. Other conditions being equal, the probability of fragmentation increases as the stability of a cluster ion decreases.

The cluster ion stability was also evaluated based on the fragmentation pattern and energy threshold of the different cluster sizes using IM-CID-MS. Taking advantage of the pressure gradient and increasing the field strength/pressure ratio in the IM-MS interface, a quick and easy way of obtaining the relative dissociation energy thresholds of the different cluster ions exiting the IM cell is provided. For field strengths between 20 and 30 V/cm, the IM-MS interface operates in a transmission-only mode and no dissociation is observed. With an increase of field strength (>30 V/cm) dissociation is observed based on *m*/*z* ion signal of fragment ions observed at the ATD of the parent ion (see Table 3). As an example, Figure 5 contains a two-dimensional IM−MS projection plot of three of the $(CsI)_nCs^+$ CID channels observed at a field strength of 40 V/cm in the IM-CID-MS; a clear separation of the parent (laser desorbed) and fragment (IM-CID-MS) ion signals is observed for $n = 2$, 4, and 5. Hereafter, since all the observed dissociation channels involve loss of CsI units, the channels will be labeled by the fragment and parent ions, i.e., $m \rightarrow n$ represents the reaction $(CsI)_mCs^+ \rightarrow (CsI)_nCs^+ + (CsI)_{m-n}$. In the inset of Figure 5 a three-dimensional IM-MS plot of the ion signal observed at $m/z = 913$ is illustrated. The most intense peak at 913 *m*/*z* corresponds to the $n = 3$ parent ion, but at longer ATD times one can also observe ion signals corresponding to the 4 → 3 and 5 → 3 reactions, which permits clear identification of the dissociation channels. Using the IM-CID-MS method, the study of the dissociation channels of a given parent ion is not affected by the other parent ions and the CID can be performed concurrently since different cluster sizes are already separated in the IM domain, unlike in other tandem MS experiments where the masses of the parent ion must be selected individually.

At a field strength of 33 V/cm, dissociation of 2 → 1 and 1 → 0 is observed, with the 2 → 1 channel being approximately one order of magnitude more abundant. Increasing the field strength to 36 V/cm, the dissociation channel of 4 → 3 is observed with dissociation of 2 → 0 and 2 → 1 as the most abundant. At 40 V/cm, the 2 → 1 and 4 → 3 channels are the most abundant and the onset of the 5 → 3 channel begins (Figure 5). At a field strength of 46 V/cm, dissociation of 3 → 1 and 3 → 0 begins. Analysis of the relative abundances of the dissociation channels shows that the fragmentation pattern of a given cluster ion is related to its predicted stability (see results in previous section, Figure 3). The cluster ions with the lowest stability, i.e., $n = 2$ and 4, dissociate at lower field strengths (33 and 36 V/cm) compared to $n = 3$ and 5 (46 and 40 V/cm) cluster ions (Table 3). Moreover, the large field strength necessary to dissociate $n = 3$ suggests it is among the most stable cluster ions.

The IM-CID-MS results were compared with high-vacuum CID MS/MS experiments, and the same trends were observed in the relative abundance of the dissociation channels, i.e., the 2 → 1 and 3 → 1 have higher fragmentation efficiency than 2 → 0 and 3 → 0, respectively. The dissociation channels for *n* larger than 3 were not observed in the high-vacuum CID MS/MS experiments due to the low desorption probability of these higher cluster ions under high-vacuum conditions (only $n = 1-3$ where observed).[4,5] A previous MS study where CsI cluster ions were generated by fast atom bombardment showed that fragmentation of $n = 6$ yields predominantly $n = 3$ using both surface-induced dissociation and 10 keV CID,[44] in agreement with the predicted stability in Figure 3. Less stable fragment ions are not as abundant in the mass spectra as they have a higher probability to experience further fragmentation because (i) they have lower energy barriers for dissociation and (ii) the amount of average internal energy they can store is smaller compared to the more stable counterparts.

TABLE 3: Dissociation Channels and Their Relative Abundances As a Function of the Field Strength in the Novel IM-CID-MS Interface

field (V/cm)	dissociation channels	%	field (V/cm)	dissociation channels	%
33	$(CsI)_1Cs^+ \rightarrow Cs^+ + CsI$	1.2%	46	$(CsI)_1Cs^+ \rightarrow Cs^+ + CsI$	7.7%
	$(CsI)_2Cs^+ \rightarrow (CsI)_1Cs^+ + CsI$	14.9%		$(CsI)_2Cs^+ \rightarrow (CsI)_1Cs^+ + CsI$	38.9%
36	$(CsI)_1Cs^+ \rightarrow Cs^+ + CsI$	1.4%		$(CsI)_2Cs^+ \rightarrow Cs^+ + (CsI)_2$	2.6%
	$(CsI)_2Cs^+ \rightarrow (CsI)_1Cs^+ + CsI$	12.8%		$(CsI)_3Cs^+ \rightarrow (CsI)_1Cs^+ + (CsI)_2$	6.1%
	$(CsI)_2Cs^+ \rightarrow Cs^+ + (CsI)_2$	0.6%		$(CsI)_3Cs^+ \rightarrow Cs^+ + (CsI)_3$	0.7%
	$(CsI)_4Cs^+ \rightarrow (CsI)_3Cs^+ + CsI$	2.8%		$(CsI)_4Cs^+ \rightarrow (CsI)_3Cs^+ + CsI$	4.0%
40	$(CsI)_1Cs^+ \rightarrow Cs^+ + CsI$	3.1%		$(CsI)_1Cs^+ \rightarrow Cs^+ + CsI$	11.5%
	$(CsI)_2Cs^+ \rightarrow (CsI)_1Cs^+ + CsI$	19.8%	50	$(CsI)_2Cs^+ \rightarrow (CsI)_1Cs^+ + CsI$	45.5%
	$(CsI)_2Cs^+ \rightarrow Cs^+ + (CsI)_2$	1.3%		$(CsI)_2Cs^+ \rightarrow Cs^+ + (CsI)_2$	2.0%
	$(CsI)_4Cs^+ \rightarrow (CsI)_3Cs^+ + CsI$	4.0%		$(CsI)_3Cs^+ \rightarrow (CsI)_1Cs^+ + (CsI)_2$	9.5%
	$(CsI)_5Cs^+ \rightarrow (CsI)_3Cs^+ + (CsI)_2$	1.3%		$(CsI)_3Cs^+ \rightarrow Cs^+ + (CsI)_3$	1.5%
43	$(CsI)_1Cs^+ \rightarrow Cs^+ + CsI$	6.8%	MS/MS[a]	$(CsI)_2Cs^+ \rightarrow (CsI)_1Cs^+ + CsI$	87%
	$(CsI)_2Cs^+ \rightarrow (CsI)_1Cs^+ + CsI$	30.8%		$(CsI)_2Cs^+ \rightarrow Cs^+ + (CsI)_2$	13%
	$(CsI)_2Cs^+ \rightarrow Cs^+ + (CsI)_2$	1.9%		$(CsI)_3Cs^+ \rightarrow (CsI)_2Cs^+ + (CsI)_1$	0%
	$(CsI)_4Cs^+ \rightarrow (CsI)_3Cs^+ + CsI$	9.0%	MS/MS[a]	$(CsI)_3Cs^+ \rightarrow (CsI)_1Cs^+ + (CsI)_2$	76%
				$(CsI)_3Cs^+ \rightarrow Cs^+ + (CsI)_3$	24%

[a] The MS/MS* results were acquired using the Applied Biosystems 4700 Mass Spectrometer. Since the parent and fragmented signals are separated in the 2D IM-MS plot, the relative abundances of a given dissociation channel (%) was computed as the ratio of the fragmented ion counts and the counts of all measured ions. In the case of the MS/MS* results, relative abundances of a given dissociation channel (%) are defined as the ratio of the fragment ion counts and the sum of all the fragment ion counts.

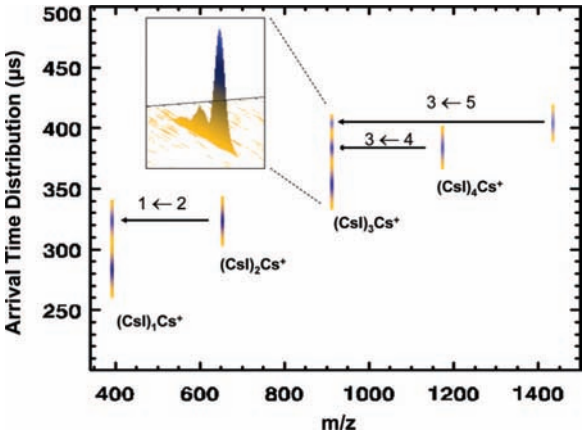

Figure 5. Two-dimensional IM-MS projection plot of the $(CsI)_nCs^+$ CID channels observed at a field strength of 40 V/cm in the IM-CID-MS. A clear separation of the parent (laser desorbed) and fragment (IM-CID-MS) ion signals is observed. (Inset) Three-dimensional IM-MS plot of the ion signal observed at $m/z = 913$ corresponding to the $n = 3$ parent ion and the $4 \rightarrow 3$ and $5 \rightarrow 3$ dissociation channels.

Unlike other studies we did not observe several dissociation channels (e.g., $3 \rightarrow 2$, $4 \rightarrow 2$, $4 \rightarrow 1$, and $4 \rightarrow 0$, etc).[45] One of the reasons could be that the threshold energies for secondary reactions are close to or even smaller than the threshold of the primary reaction. For example, the lack of evidence for the $3 \rightarrow 2$ channel can be attributed to the higher efficiency of the $2 \rightarrow 1$ channel at 46 V/cm (lower threshold than $3 \rightarrow 2$), i.e., the reaction occurs via a succession of collisional activation events with 2* as short-lived intermediate ($3 \rightarrow 2^* \rightarrow 1$), leading to the observation of only the $3 \rightarrow 1$ channel. This in agreement with the high-vacuum CID MS/MS experiments and previously reported breakdown curves showing $3 \rightarrow 1$ as the lowest energy channel.[45] Moreover, it was suggested that the reaction $3 \rightarrow 0$ occurs as $3 \rightarrow 1^* \rightarrow 0$,[45] which is in agreement with the relative efficiencies observed at 46 V/cm in IM-CID-MS. For $n \geq 4$, no observation of other channels is probable because (i) there is an inadequate abundance of the parent ion and (ii) there is not sufficient energy to achieve fragmentation. For example, we only observed the lowest energy channel for $n = 4$ ($4 \rightarrow 3$); the threshold energies for the dissociation channels of $n = 4$ are related as $(4 \rightarrow 3) < (4 \rightarrow 1) < (4 \rightarrow 2) < (4 \rightarrow 0)$, i.e., a larger energy is necessary to observe the channels $4 \rightarrow 1$, $4 \rightarrow 2$, and $4 \rightarrow 0$.[45] In the same manner, we only observed the lowest energy channel for $n = 5$ ($5 \rightarrow 3$); the threshold energies for the dissociation channels of $n = 5$ are related as $(5 \rightarrow 3) < (5 \rightarrow 1) < (5 \rightarrow 4) < (5 \rightarrow 2) < (5 \rightarrow 0)$.[45]

Conclusions

The pulsed-UV laser IM-CID-MS experiment permits characterization of gas-phase cluster ions by their CCS (gas-phase packing density) and dissociation channels (energy criterion). The experimental results of the $(CsI)_nCs^+$ ($n = 0-7$) cluster ions show a good separation in both ion mobility and mass-to-charge domains permitting a clear identification based on size (gas-phase packing density) and mass. The theoretical CCS data for the lowest energy isomers (i.e., more stable structures) shows a better agreement with the experimental values compared to the higher energy isomers. Sixteen lowest energy candidate structures were found in the search performed at the DFT/B3LYP/LACV3P** and MP2/LACV3P** levels, and a good description of the candidate relative stability is obtained by the D-plot methodology.

The gas-phase cluster ion stability was investigated experimentally using ion−neutral collisional activation in both the IM cell and the IM-CID-MS. The stability analysis and field strength dependence on the ion abundances show that the fragmentation inside the IM cell can be related to the cluster ion stabilities: the $(CsI)_nCs^+$ cluster ion with $n = 2$ exhibit the lowest stability and the lowest abundance in the IM spectra at the higher IM field strengths investigated (>30 V cm^{-1} Torr^{-1}). The IM-CID-MS configuration allowed us to perform dissociation studies of mobility separated ion packets exiting the IM cell, and the relative probability of the dissociation channels observed is in good agreement with the theoretical stability analysis, i.e., the cluster ion with sizes $n = 2$ and 4 present a

larger fragmentation probability owing to a lower stability. The higher predicted stability for $n = 3$ and 7 agrees with the relative higher energy threshold for dissociation in the IM-CID-MS and the relative higher ion abundances observed in MS experiments.[8]

Acknowledgment. The authors would like to acknowledge the Brazilian Agencies CNPq, Faperj, Instituto do Milênio de Materiais Complexos, the U.S. Department of Energy, Division of Chemical Science, BES, and the R. A. Welch Foundation for their financial support.

References and Notes

(1) Barlak, T. M.; Campana, J. E.; Colton, R. J.; DeCorpo, J. J.; Wyatt, J. R. *J. Phys. Chem.* **1981**, *85*, 3840.
(2) Barlak, T. M.; Wyatt, J. R.; Colton, R. J.; DeCorpo, J. J.; Campana, J. E. *J. Am. Chem. Soc.* **1982**, *104*, 1212.
(3) Campana, J. E.; Barlak, T. M.; Colton, R. J.; DeCorpo, J. J.; Wyatt, J. R.; Dunlap, B. I. *Phys. Rev. Lett.* **1981**, *47*, 1046.
(4) Collado, V. M.; Fernández-Lima, F. A.; Ponciano, C. R.; Nascimento, M. A. C.; Velazquez, L.; Silveira, E. F. d. *Phys. Chem. Chem. Phys.* **2005**, *7*, 1971.
(5) Fernández-Lima, F. A.; Collado, V. M.; Ponciano, C. R.; Farenzena, L. S.; Pedrero, E.; Silveira, E. F. D. *Appl. Surf. Sci.* **2003**, *217*, 202.
(6) Fernandez-Lima, F. A.; Ponciano, C. R.; Filho, H. D. F.; Pedrero, E.; Chaer Nascimento, M. A.; da Silveira, E. F. *Appl. Surf. Sci.* **2006**, *252*, 8171.
(7) Twu, Y. J.; Conover, C. W. S.; Yang, Y. A.; Bloomfield, L. A. *Phys. Rev. B* **1990**, *42*, 5306.
(8) Pflaum, R.; Sattler, K.; Recknagel, E. *Phys. Rev. B* **1986**, *33*, 1522.
(9) Wang, G.; Cole, R. B. *Anal. Chem.* **1998**, *70*, 873.
(10) Ens, W.; Beavis, R.; Standing, K. G. *Phys. Rev. Lett.* **1983**, *50*, 27.
(11) Ellis, H. W.; McDaniel, E. W.; Albritton, D. L.; Viehland, L. A.; Lin, S. L.; Mason, E. A. *Atomic Data Nuclear Data Tables* **1978**, *22*, 179.
(12) Ellis, H. W.; Thackston, M. G.; McDaniel, E. W.; Mason, E. A. *Atomic Data Nuclear Data Tables* **1984**, *31*, 113.
(13) Jarrold, M. F.; Bower, J. E. *Chem. Phys. Lett.* **1988**, *149*, 433.
(14) Shelimov, K. B.; Hunter, J. M.; Jarrold, M. F. *Int. J. Mass Spectrom. Ion Process.* **1994**, *138*, 17.
(15) Dugourd, P.; Hudgins, R. R.; Jarrold, M. F. *Chem. Phys. Lett.* **1997**, *267*, 186.
(16) Fye, J. L.; Jarrold, M. F. *Int. J. Mass Spectrom.* **1999**, *185*−*187*, 507.
(17) Lerme, J.; Dugourd, P.; Hudgins, R. R.; Jarrold, M. F. *Chem. Phys. Lett.* **1999**, *304*, 19.
(18) Shvartsburg, A. A.; Jarrold, M. F. *Chem. Phys. Lett.* **2000**, *317*, 615.
(19) Radi, P. P.; Hsu, M.-T.; Rincon, M. E.; Kemper, P. R.; Bowers, M. T. *Chem. Phys. Lett.* **1990**, *174*, 223.
(20) von Helden, G.; Gotts, N. G.; Maitre, P.; Bowers, M. T. *Chem. Phys. Lett.* **1994**, *227*, 601.
(21) von Helden, G.; Gotts, N. G.; Palke, W. E.; Bowers, M. T. *Int. J. Mass Spectrom. Ion Process.* **1994**, *138*, 33.
(22) Zhang, Q.; Kemper, P. R.; Bowers, M. T. *Int. J. Mass Spectrom.* **2001**, *210*−*211*, 265.
(23) Maier-Borst, M.; Loffler, P.; Petry, J.; Kreisle, D. *Z. Phys. D* **1997**, *40*, 476.
(24) Tabrizchi, M. *Anal. Chem.* **2003**, *75*, 3101.
(25) Martin, T. P. *Phys. Rep.* **1983**, *95*, 167.
(26) Welch, D. O.; Lazareth, O. W.; Dienes, G. J.; Hatcher, R. D. *J. Chem. Phys.* **1976**, *64*, 835.
(27) Hwang, H. J.; Sensharma, D. K.; El-Sayed, M. A. *J. Phys. Chem.* **1989**, *93*, 5012.
(28) Diefenbach, J.; Martin, T. P. *J. Chem. Phys.* **1985**, *83*, 4585.
(29) Phillips, N. G.; Conover, C. W. S.; Bloomfield, L. A. *J. Chem. Phys.* **1991**, *94*, 4980.
(30) Xiuling, L.; Robert, L. W. *J. Chem. Phys.* **1993**, *98*, 6170.
(31) Fatemi, D. J.; Fatemi, F. K.; Bloomfield, L. A. *Phys. Rev. A* **1996**, *54*, 3674.
(32) Antoine, R.; Ph, D.; Rayane, D.; Benichou, E.; Broyer, M. *J. Chem. Phys.* **1997**, *107*, 2664.
(33) Luaña, V.; Pueyo, L. *Phys. Rev. B* **1990**, *41*, 3800.
(34) Aguado, A.; Ayuela, A.; L'Opez, J. M.; Alonso, J. A. *J. Phys. Chem. B* **1997**, *101*, 5944.
(35) Aguado, A.; Ayuela, A.; López, J. M.; Alonso, J. A. *Phys. Rev. B* **1997**, *56*, 15353.
(36) Aguado, A.; Ayuela, A.; López, J. M.; Alonso, J. A. *Phys. Rev. B* **1998**, *58*, 9972.
(37) Ochsenfeld, C.; Ahlrichs, R. *J. Chem. Phys.* **1994**, *101*, 5977.
(38) Ochsenfeld, C.; Gauss, J.; Ahlrichs, R. *J. Chem. Phys.* **1995**, *103*, 7401.
(39) Fernández-Lima, F. A.; Ponciano, C. R.; Silveira, E. F. D.; Nascimento, M. A. C. *Chem. Phys. Lett.* **2007**, *445*, 147.
(40) Fernandez-Lima, F. A.; Ponciano, C. R.; Faraudo, G. S.; Grivet, M.; da Silveira, E. F.; Nascimento, M. A. C. *Chem. Phys.* **2007**, *340*, 127.
(41) Fernández-Lima, F. A.; Cardozo, T. M.; Rodriguez, R. M.; Ponciano, C. R.; Silveira, E. F. D.; Nascimento, M. A. C. *J. Phys. Chem. A* **2007**, *111*, 8302.
(42) Fernández-Lima, F. A.; Ponciano, C. R.; Silveira, E. F. d.; Nascimento, M. A. C. *Chem. Phys. Lett.* **2006**, *426*, 351.
(43) Fernández-Lima, F. A.; Ponciano, C. R.; Nascimento, M. A. C.; Silveira, E. F. D. *J. Phys. Chem. A* **2006**, *110*, 10018.
(44) Nikolaev, E. N.; Somogyi, A.; Smith, D. L.; Gu, C.; Wysocki, V. H.; Martin, C. D.; Samuelson, G. L. *Int. J. Mass Spectrom.* **2001**, *212*, 535.
(45) Herzschuh, R.; Drewello, T. *Int. J. Mass Spectrom.* **2004**, *233*, 355.
(46) Stone, E. G.; Gillig, K. J.; Ruotolo, B. T.; Russell, D. H. *Int. J. Mass Spectrom.* **2001**, *212*, 519.
(47) Ruotolo, B. T.; Gillig, K. J.; Stone, E. G.; Russell, D. H.; Fuhrer, K.; Gonin, M.; Schultz, J. A. *Int. J. Mass Spectrom.* **2002**, *219*, 253.
(48) Gillig, K. J.; Ruotolo, B. T.; Stone, E. G.; Russell, D. H. *Int. J. Mass Spectrom.* **2004**, *239*, 43.
(49) McDaniel, E. W.; Mason, E. A. *Mobility and diffusion of ions in gases*; John Wiley and Sons, Inc.: New York, 1973.
(50) Mesleh, M. F.; Hunter, J. M.; Shvartsburg, A. A.; Schatz, G. C.; Jarrold, M. F. *J. Phys. Chem.* **1996**, *100*, 16082.
(51) Shvartsburg, A. A.; Jarrold, M. F. *Chem. Phys. Lett.* **1996**, *261*, 86.
(52) Watts, P.; Wilders, A. *Int. J. Mass Spectrom. Ion Process.* **1992**, *112*, 179.
(53) Hay, P. J.; Wadt, W. R. *J. Chem. Phys.* **1985**, *82*, 299.
(54) *Jaguar 6.0 manual*; Schroedinger Inc.: Portland, OR, 2004.
(55) Mesleh, M. F.; Hunter, J. M.; Shvartsburg, A. A.; Schatz, G. C.; Jarrold, M. F. *J. Phys. Chem.* **1996**, *100*, 16082.
(56) Kinsel, G. R.; Russell, D. H. *J. Am. Soc. Mass Spectrom.* **1995**, *6*, 619.
(57) Verbeck, G. F.; Ruotolo, B. T.; Gillig, K. J.; Russell, D. H. *J. Am. Soc. Mass Spectrom.* **2004**, *15*, 1320.
(58) Notker, R.; Trickey, S. B. *J. Chem. Phys.* **1997**, *106*, 8940.
(59) Curt, M.; Breneman, K. B. W. *J. Comput. Chem.* **1990**, *11*, 361.

JP8047086